33RD CONGRESS
OF THE INTERNATIONAL COUNCIL
OF THE AERONAUTICAL SCIENCES
STOCKHOLM, SWEDEN, 4–9 SEPTEMBER, 2022

ICAS 2022 SWEDEN

Research on the ductile fracture of AL7085 and TC11 under complex stress state

Y. J. Liu[1]

[1] AVIC the First Aircraft Institute

Abstract

In this paper, ductile fracture behaviors of aluminon alloy AL7085 and titanium alloy TC11 under complex stress state are experimentally and numerically studied. Based on coupon tests and simulations, the curves of fracture strain-triaxiality are obtained and used as fracture criteria of AL7085 and TC11. The experimental and numerical studies of joint structure are made to verify the fracture criteria.

Keywords: complex stress state; coupon tests; joint structure; ductile fracture; FEM simulation

1. Introduction

It is difficult to accurately predict the load capacity and failure behavior of aircraft structure with current engineering design method due to the complicity of structure details and loading conditions. It becomes a significant method to aid structure design and strength analysis by using FE simulation in aircraft design engineering [1-3].

Previous experiments have revealed that metal under complex stress state has a significantly different fracture behavior compared with it under simple uniaxial or biaxial stress states [4-10]. The triaxiality is one of the most important stress state parameters that have obvious effects on the ductile fracture of metal [11-15]. For the critical components of aircraft, such as joint structures, the complicate details and loading conditions make these structures under complex 3D stress states. In order to achieve a safe, reliable and efficient structure design, it is important to have a good understand of the fracture behavior of material, especially under complex stress state.

The aluminon and titanium alloys are the metals widely used in aircraft structure. In this paper, ductile fracture behaviors of aluminon alloy AL7085 and titanium alloy TC11 under complex stress state are experimentally and numerically studied. Firstly, several types of coupon tests are designed and conducted to obtain the fracture data of material under different stress states, i.g. the triaxiality. Secondly, combining the coupon tests and simulations, the curves of fracture strain-triaxiality are established which can be used as the fracture criteria. Thirdly, in order to verify the accuracy of fracture criterion, experiments of joint structure are conducted as well as the fracture simulations.

2. Coupon tests of complex stress state

In order to access fracture behavior under different stress state, such as triaxiality, the coupon tests are designed in this paper, which includes cylinder compression tests with different length-radius ratio, plate tension-shear tests with different grooved angles, round bar tension tests with different notched radius. The coupon specimens are shown in Fig.1 and the implementations are shown in Fig. 2. Those coupon tests widely cover the different range of triaxiality illustrated in Fig. 3. Triaxiality is denoted as the ratio of mean stress and equivalent stress,

$$\eta = \frac{\sigma_m}{\sigma_{eq}}, \tag{1}$$

where σ_m is the mean stress, σ_{eq} is the equivalent stress.

Although the initial triaxiality value of some coupons with simple geometry can be theoretically calculated [16], the actual triaxiality of the presented coupons depend on their size of details, deformations, and can be only obtained by FE analysis. It should be noted that the cylinder coupon is not under exact uniaxial compression because of the friction existing on the surface between coupon and fixture. It makes the cylinder become “drum shape” on the loading process. So, the actual stress state at position of crack is the combination of compression and shear when fracture occurs.

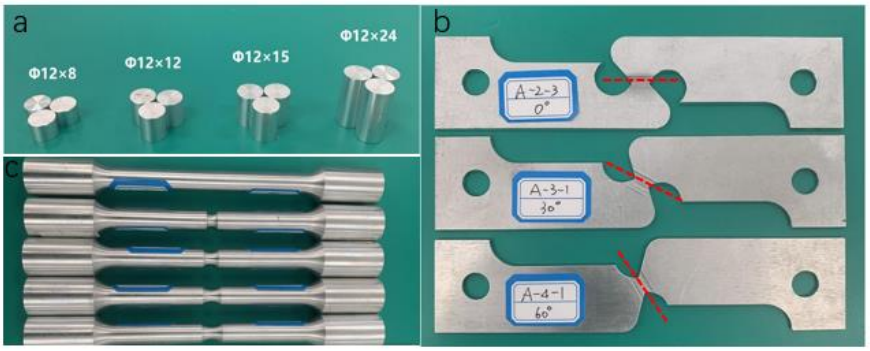

Fig.1 coupon specimens of cylinder compression tests (a), plate tension-shear tests (b), smooth and notched bar tension tests (c).

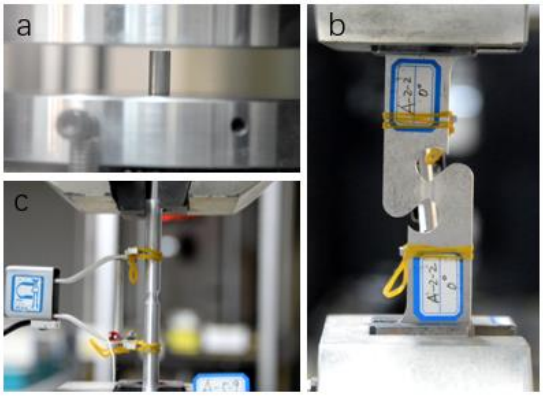

Fig.2 The implementation of cylinder compression test (a), plate tension-shear test (b), smooth and notched bar tension test (c).

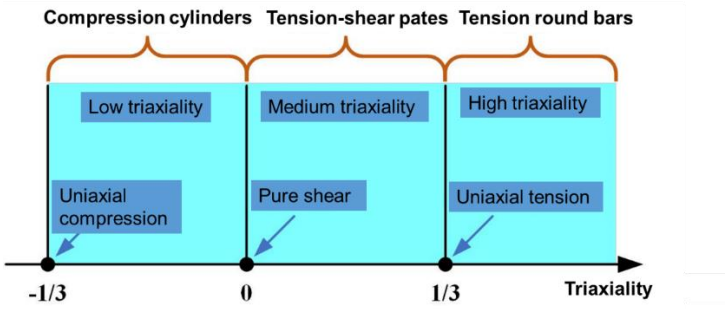

Fig.3 The range of the triaxiality of different coupon tests.

The force-displacement curves are obtained from those coupon tests, especially the displacement when fracture occurs. Then, combined with coupon test simulations, the actual triaxiality and plastic strain at the displacement when fracture occurs can be obtained and the fracture starin-triaxiality curve can be estabilished.

3. Fracture behaviors of AL7085 and TC11 under complex stress state

3.1 Material constants of AL7085 and TC11

In order to conduct coupon test simulations, the material constants of AL7085 and TC11 should be first adopted according to the tension test of smooth round bar.

In this paper, the Johnson-Cook constitutive model, $\sigma=A+B\left(\varepsilon^{p}\right)^{n}$, is used. The material constants of AL7085 and TC11 are listed in Table 1.

Table 1 the material constants of AL7085 and TC11

Material	Elastic constants		Johnson-Cook constitutive relation		
	E（MPa）	Poisson's ratio	A （MPa）	B （MPa）	n
AL7085	67100	0.33	450	496	0.56
TC11	118700	0.33	954	629	0.44

3.2 fracture strain-triaxiality relations of AL7085 and TC11

According to coupon test simulations, the internal data pairs of plastic strain and triaxiality are listed in Table 2 and Table 3 for AL7085 and TC11. It reveals that fracture behavior of AL7085 and TC11 are significantly different.

Table 2 the fracture strain-triaxiality data of coupon test of AL 7085

Tests	Sizes	Triaxiality	Fracture strain
Cylinder compression tests	Φ12×24	-0.294	0.459
	Φ12×15	-0.245	0.241
	Φ12×12	-0.195	0.192
	Φ12×8	-0.177	0.155
Plate tension-shear tests	0°	0.107	0.127
	30°	0.217	0.038
	60°	0.383	0.147
Round bar tension tests	Smooth	0.337	0.0447
	Notched radius 3mm	0.469	0.0362
	Notched radius 5mm	0.573	0.0314
	Notched radius 7mm	0.600	0.0312
	Notched radius 9mm	0.672	0.0294

Table 3 the fracture strain-triaxiality data of coupon test of TC11

Tests	Sizes	Triaxiality	Fracture strain
Cylinder compression tests	Φ12×24	-0.294	0.316
	Φ12×15	-0.245	0.256
	Φ12×12	-0.195	0.205
	Φ12×8	-0.177	0.188
Plate tension-shear tests	0°	0.107	0.147
	30°	0.217	0.153
	60°	0.383	0.198
Round bar tension tests	Smooth	0.337	0.204
	Notched radius 3mm	0.469	0.0973
	Notched radius 5mm	0.573	0.0889
	Notched radius 7mm	0.600	0.0810
	Notched radius 9mm	0.672	0.0791

The AL7085 shows a monotonous decreasing fracture strain as the triaxiality increases. The curve of fracture strain-triaxiality is drawn in Fig. 4, which is well fitted by Johnson-Cook model,

$$\varepsilon_f^p = 0.047 + 0.013\exp(-11.59\eta), \tag{2}$$

where ε_f^p is fracture strain, η is triaxiality. It reveals that the AL7085 tends to fracture at high triaxiality stress state.

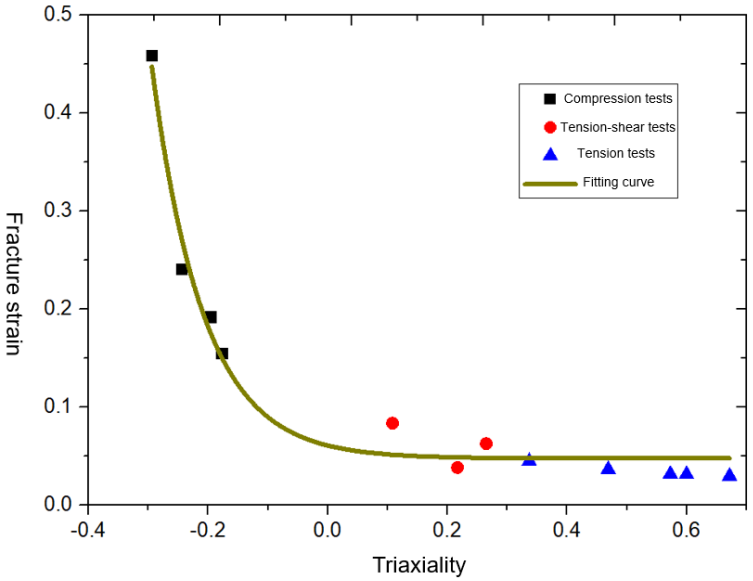

Fig. 4 The fracture strain-triaxiality curve of AL7085.

However, the TC11 shows a non-monotonous behavior that fracture strain has a local minimum around shear stress state. The curve of fracture strain-triaxiality is drawn in Fig. 5, which is fitted by straight line in low triaxiality region, by quadratic polynomial in medium triaxiality region and by Johnson-Cook model in high triaxiality region.

$$\varepsilon_f^p = \begin{cases} 0.089 - 0.75\eta & -1/3 < \eta \le -0.11 \\ 0.15 - 0.13\eta + 0.64\eta^2 & -0.11 < \eta \le 1/3 \\ 0.082 + 606.11\exp(-22.22\eta) & \eta > 1/3 \end{cases}. \tag{3}$$

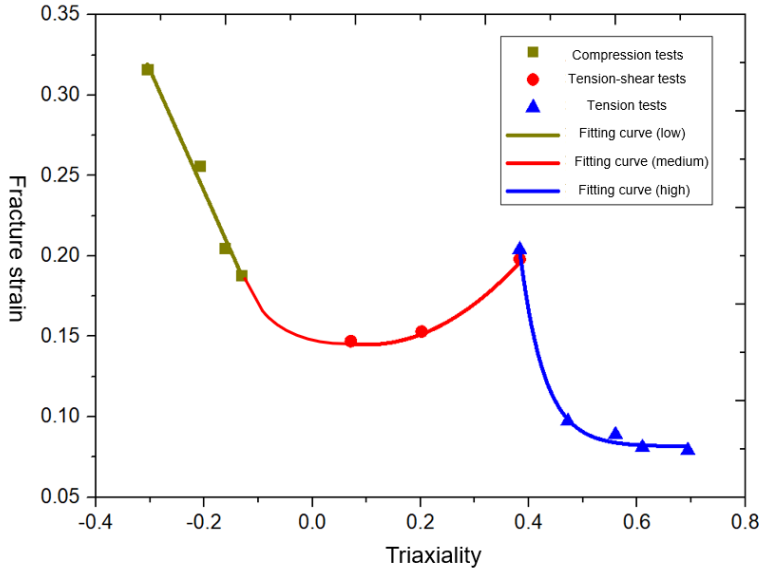

Fig. 5 The fracture strain-triaxiality curve of TC11.

It shows “hollows” in both medium and high triaxiality stress states, which means that it is easier to fracture at shear dominant stress state and 3D tension stress state.

The obtained fracture strain-triaxiality curves can be used as fracture criteria of AL7085 and TC11 in numerical simulation. And incorporated with damage accumulation, the progressive failure analysis can be conducted to predict the fracture behavior of structure.

In numerical simulation, the damage is defined as

$$D=\int_0^{\varepsilon_f}\frac{1}{\varepsilon_f^p(\eta)}d\varepsilon^p\,. \tag{4}$$

When the damage accumulates to unity, the crack is formed and the element is “deleted” from the FE model.

4. Numerical verification of joint structure experiment

Furthermore, in order to verify the ductile fracture criterion of AL7085 and TC11, the fracture experiments of a joint structure (Fig.6) are conducted as well as their numerical simulation applied with the ductile fracture criteria above. The joint structure is fixed on the test fixture through bolts at the corners and loaded in the direction as seen in the Fig. 7.

The joint structures of the AL7085 and TC11 are both fractured in lug region shown in Fig. 8 and 9, in which the arrow line indicates the loading direction. However, their failure modes are obviously different. The AL7085 joint has a tension failure mode (Fig. 8), while the TC11 joint has a shear failure mode (Fig. 9). Since the joints of AL7085 and TC11 have the same stress distribution, the difference of their failure modes reveals that the 3D stress state has significant impact on the fracture behavior of different materials. It is not capable to accurately predict the fracture behavior under complex stress state by using the traditional forth strength theory of ultimate stress of material, i.e. $\sigma_{eq}=\sigma_b$.

Meanwhile, the progressive failure analysis of the joint structure is performed on the ABAQUS/Explicit by using VUMAT user’s subroutine. In simulation, the linear damage accumulation is adopted. When the damage value accumulates to unity, the element is ’deleted’ and the crack is formed. The comparisons between experiments and simulations show good convergence in fracture modes (Fig. 8 and 9) and high accuracy in load capacity (Fig. 10) for both AL7085 and TC11 joints.

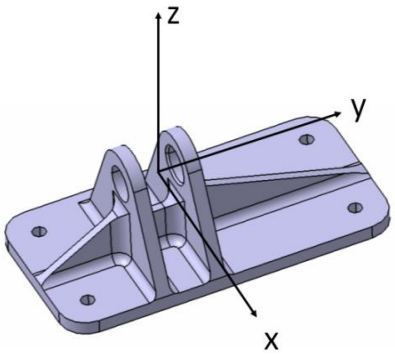

Fig.6 The layout of joint structure.

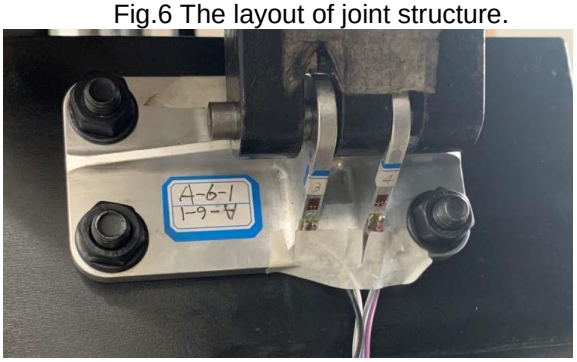

Fig. 7 The illustrations of test fixture, constraint and loading condition.

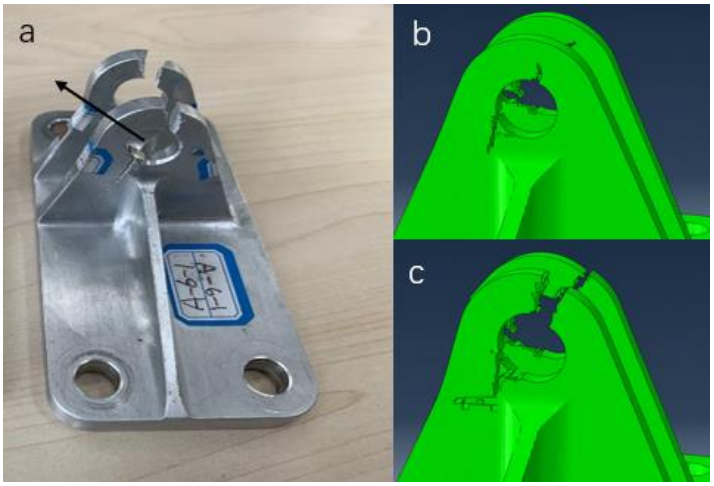

Fig. 8 The fracture of AL7085 joint of experimental result (a) and simulations of crack initiation (b) and propagation(c)

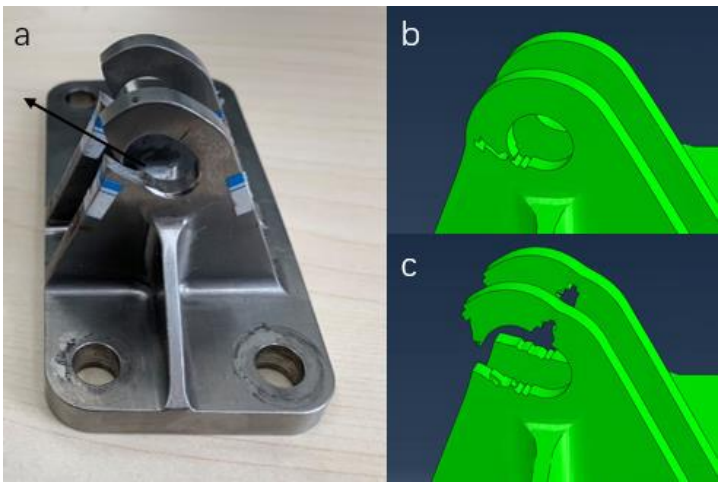

Fig. 9 The fracture of TC11 joint of experimental result (a) and simulations of crack initiation (b) and propagation (c).

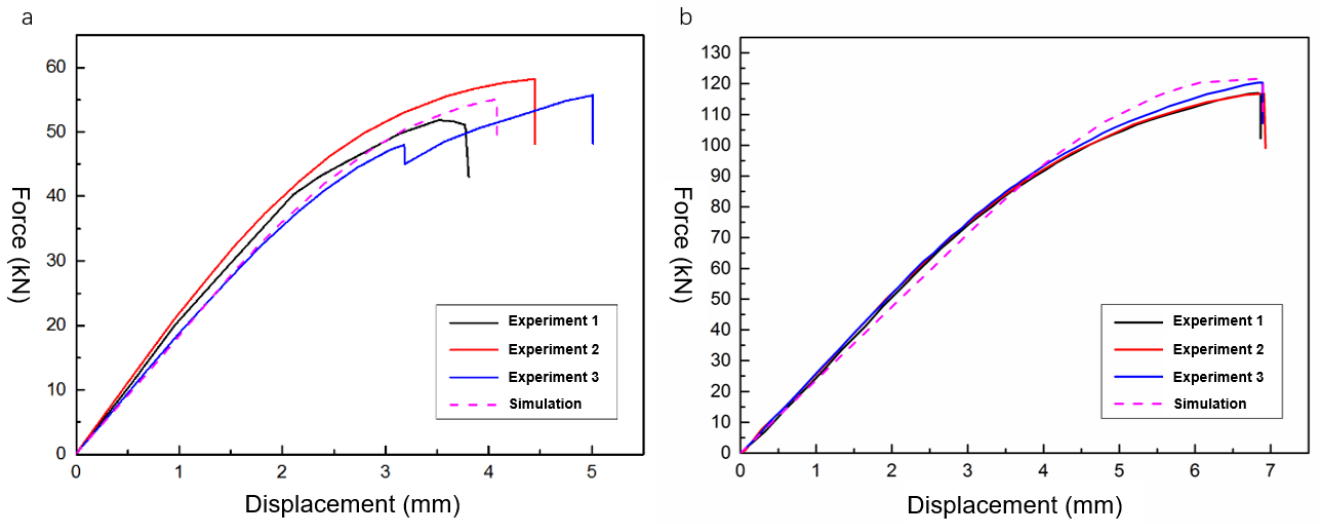

Fig. 10 The force-displacement curve of joint test and simulation of AL7085 (a) and TC11 (b).

5. Conclusions

In this paper, combining both experimental and numerical methods, the ductile fracture behaviors of aluminon alloy AL7085 and titanium alloy TC11 under complex stress state are studied through a series of coupon tests, including cylinder compression tests with different length-radius ratio, plate tension-shear tests with different grooved angles, round bar tension tests with different notched radius. Based on the fracture tests and corresponding simulations, the curves of fracture strain-triaxiality of AL7085 and TC11 are obtained as fracture criteria of material under complex stress states.

The fracture strain-triaxiality curves of AL7085 and TC11 are obviously different. The curve of AL7085 shows a monotonous decreasing fracture strain as the parameter of triaxiality increases, which means it tends to fracture at 3D tension stress state. However, the curve of TC11 shows “hollows” in both medium and high triaxiality stress states, which means that it easily fractures at both shear dominant stress state and 3D tension stress state. It implies that structures of both materials have totally different fracture behaviors under complex stress states.

To verify the obtained fracture criteria of AL7085 and TC11, the experimental and numerical studies of joint structure are conducted. It shows that the numerical results agree very well with experimental result both in fracture modes and ultimate loading capacity.

References

[1] Gavrylov I, Karuskevich M, Ignatovich S, et al. Influence of corrosion preventive compounds on the friction force in aircraft lap joints. Fatigue and Fracture of Engineering Materials and Structures, Vol. 45, No. 3, pp 938-941, 2022.

[2] Andrzej, Leski. Numerical calculation of the aircraft skin with multi-site damage. Research Works of Air Force Institute of Technology, Vol. 25, No.1, pp 37-47, 2009.

[3] Zimmermann N, Wang P H. A review of failure modes and fracture analysis of aircraft composite materials. Engineering Failure Analysis, Vol. 115, pp 104692, 2020.

[4] Yu M H. Advances in strength theories for materials under complex stress state in the 20th Century. Applied Mechanics Reviews, ASME, Vol. 55, No. 3, pp169-218, 2002.

[5] Xue L. Damage accumulation and fracture initiation in uncracked ductile solids subject to triaxial loading. International Journal of Solids and Structures, Vol. 44, pp 5163–5181, 2007.

[6] Bai Y, Wierzbicki T. A new model of metal plasticity and fracture with pressure and Lode dependence. International Journal of Plasticity, Vol. 24, pp 1071–1096, 2008.

[7] Gao X, Zhang T, Hayden M, et al. Effects of the stress state on plasticity and ductile failure of an aluminum 5083 alloy. International Journal of Plasticity, Vol. 25, No. 12, pp 2366-2382, 2009.

[8] Wierzbicki T, Bao Y, Lee Y W, et al. Calibration and evaluation of seven fracture models. International Journal of Mechanical Sciences, Vol. 47, No. 4–5, pp 719-743, 2005.

[9] Kornev, V M, Kurguzov, V D. Multiparametric sufficient criterion of quasi-brittle fracture for complicated stress state. Engineering Fracture Mechanics, Vol. 75, No. 5, pp 1099-1113, 2008.

[10] Tretyakova T V , Mugatarov, A I, & Feklistova, E V. Experimental study of macroscopic localization of plastic flow in al-mg alloy under complicated stress-strain state. IOP Conference Series: Materials Science and Engineering, Vol. 747, No. 1, 012132 (7pp), 2020.

[11] Bai Y, Wierzbicki T. A comparative study of three groups of ductile fracture loci in the 3D space. Engineering Fracture Mechanics, Vol. 135, pp 147-167, 2015.

[12] Johnson G R, Cook W H. Fracture characteristics of three metals subjected to various strains, strain rates, temperatures and pressures. Engineering Fracture Mechanics, Vol. 21, No. 1, pp 31-48, 1985.

[13] Tvergaard V, Needleman A. A Analysis of the cup-cone fracture in a round tensile bar. Acta Metallurgica, Vol. 32, pp 157-189, 1984.

[14] Liu Y J, Sun Q, Fan X L, Suo T. A stress-invariant based multi–parameters ductile progressive fracture model. Mat. Sci. Materials Science & Engineering A, Vol. 576, No. 1, pp 337–345, 2013.

[15] Liu Y J, Sun Q. A dynamic ductile fracture model on the effects of pressure, Lode angle and strain rate. Materials Science & Engineering A, Vol. 589, pp 262–270, 2014.

[16] Bridgman P W. Studies in Large Plastic Flow and Fracture. McGraw-Hill, 1952.

Copyright Statement